Brewer's spent grains as biofuels in combustion-based energy recovery processes: Evaluation of thermo-oxidative decomposition

O. Gil-Castell, N. Mascia, C. Primaz, F. Vásquez-Garay, M.G. Baschetti, A. Ribes-Greus. Brewer's spent grains as biofuels in combustion-based energy recovery processes: Evaluation of thermo-oxidative decomposition. Fuel, 2022; 312(122955)

Brewer's spent grains as biofuels in combustion-based energy recovery processes: Evaluation of thermo-oxidative decomposition

O. Gil-Castell[1], N. Mascia[2], C. Primaz[1], F. Vásquez-Garay[3], M.G. Baschetti[2], A. Ribes-Greus[1,*]

1. Instituto de Tecnología de Materiales (ITM), Universitat Politècnica de València (UPV), Camino de Vera S/n, 46022, Valencia, Spain.
2. Dipartimento di Ingegneria Civile, Chimica, Ambientale e dei Materiali (DICAM), Alma Mater Studiorum – Università di Bologna, Via Terracini, 28, 40131 Bologna, Italy
3. Centro de Excelencia en Nanotecnología (CEN), LEITAT Chile, Román Díaz 532, Providencia, Santiago, Chile

*Corresponding author: aribes@ter.upv.es

O. Gil-Castell, N. Mascia, C. Primaz, F. Vásquez-Garay, M.G. Baschetti, A. Ribes-Greus. Brewer's spent grains as biofuels in combustion-based energy recovery processes: Evaluation of thermo-oxidative decomposition. Fuel, 2022; 312(122955)

Brewer's spent grains as biofuels in combustion-based energy recovery processes: evaluation of thermo-oxidative decomposition

O. Gil-Castell[1], N. Mascia[2], C. Primaz[1], F. Vásqez-Garay[3], M. G. Baschetti[2], A. Ribes-Greus[1,*]

[1]Instituto de Tecnología de Materiales (ITM), Universitat Politècnica de València (UPV). Camino de Vera s/n, 46022 Valencia, Spain.

[2]Dipartimento di Ingegneria Civile, Chimica, Ambientale e dei Materiali (DICAM), Alma Mater Studiorum – Università di Bologna. Via Terracini, 28, 40131, Bologna, Italy.

[3]Centro de Excelencia en Nanotecnología (CEN), LEITAT Chile, Román Díaz 532, Providencia, Santiago, Chile

[*]Corresponding author:

A. Ribes-Greus aribes@ter.upv.es

Graphical abstract

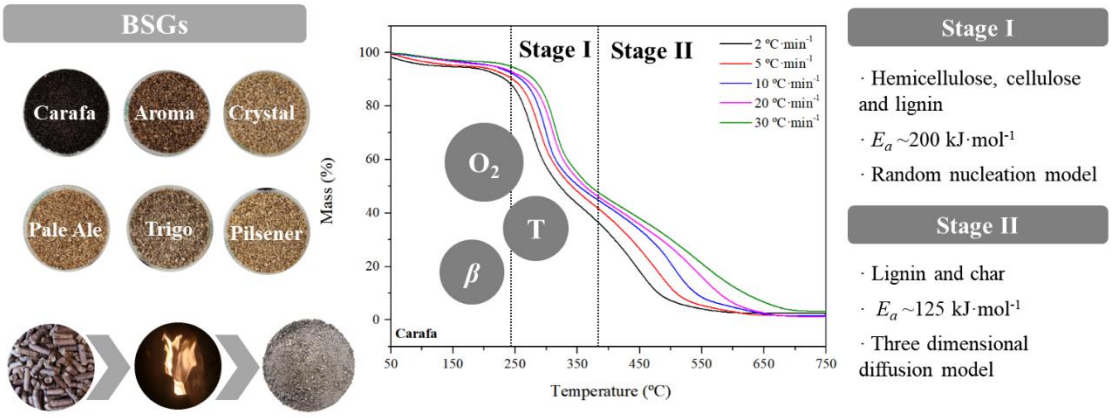

Abstract

The high global generation of wastes and side streams from agri-food production has led to environmental impact and causes nature degradation due to their uncontrolled management. These wastes are profitable materials with significant economic value that could otherwise be exploited as new sources in the feed industry or the production of bioenergy. Among them, brewer's spent grain (BSG) is a solid by-product generated in the beer-brewing process that consists of the barley grain husks together with parts of the pericarp and seed coat layer. Although it is rich in fibres and proteins, its main use is currently limited to animal feed or simply deposition to landfills. This study pursues the evaluation of BSGs as biofuels in energy recovery processes. For this purpose, the elemental composition, the higher heating value, the content of volatiles, fixed carbon, moisture, and ash yield along with the kinetic analysis of its decomposition during thermo-oxidative combustion were assessed. The thermo-oxidative decomposition of hemicellulose, cellulose, lignin, and char occurred in two main stages. The average apparent activation energy for Stage I was 190-200 $kJ \cdot mol^{-1}$, significantly higher than that of Stage II (100-150 $kJ \cdot mol^{-1}$). Stage I revealed a random nucleation kinetic model (F_n) and involved the volatilisation of hemicellulose and cellulose and partially lignin. Stage II, described by a three-dimensional diffusion kinetic model (D_4), comprised the completion of lignin and the decomposition of char. The environmental advantage of using such residues was demonstrated with the low ash yield (in the range of 1.7-5.4%) and high calorific value between 17.8 and 19.1 $MJ \cdot kg^{-1}$. The obtained results serve as the baseline for describing the energy recovery process in a reactor that uses BSG residues as feedstock under oxidative conditions. Altogether it is pointed out the feasibility of using pelletised BSGs regardless of the malt type or mixture as a renewable source of energy in incineration plants above 500 ºC.

Keywords

Biomass, valorisation, renewable energy, kinetic analysis, activation energy

1. Introduction

Biomass can be defined as any hydrocarbon material source, including natural and derived structures, such as woody and herbaceous species, woody wastes, agricultural and industrial residues, waste paper, municipal solid waste, sawdust, grass, waste from food processing, animal wastes, aquatic plants and industrial and energy crops [1]. It has a complex chemical composition, of which organic and inorganic constituents are important for further conversion processes. The leading compounds of vegetal biomass are cellulose, hemicellulose, and lignin. Moreover, it also includes extractives, that are non-structural compounds, mostly soluble in water and/or numerous organic solvents such as fatty acids, lipids, terpenoids, phenolic compounds, glycosides, proteins, triglycerides, terpenes, waxes, cutin, suberin, flavonoids, betalains, or alkaloids [2–4].

Among the main uses of biomass, special interest is given to the production of energy [5,6]. Most of the energy produced from biomass comes from wood and wood wastes (64%), followed by solid waste (24%), agricultural waste (6%), and landfill gases (6%). There are several benefits of employing biomass for energy generation and biofuels production such as environmental, economic, social, or energetic. The use of biomass for the production of bioenergy can help to reduce greenhouse gases, contribute to the growth of healthier forests, enhance rural economies, and decrease the dependency on foreign oil [7].

In the last years, agri-food and agricultural residues have emerged as suitable feedstock for energy recovery processes due to their capacity in energy production [8]. Their high production rates and the necessity of suitable management have pointed them out as a feasible alternative to traditional fuels [9]. For being suitable for energetic valorisation,

calorific values above 15 $MJ \cdot kg^{-1}$ and a maximum degree of humidity from 10 to 15% is required [10].

The brewery industry gives a huge contribution to agri-food biomass production. Beer is one of the oldest and most widely consumed alcoholic drinks in the world, and the third most popular drink overall after water and tea. The beer production industry generates four main solid wastes: the brewer's spent grain (BSG) derived from the grain processing, hot trub (protein coagulation that occurs during the boiling of the wort), residual brewer's yeast (microbial fermentative activity), and the diatomaceous earth (the result of the beer clarification process), according to **Figure 1**.

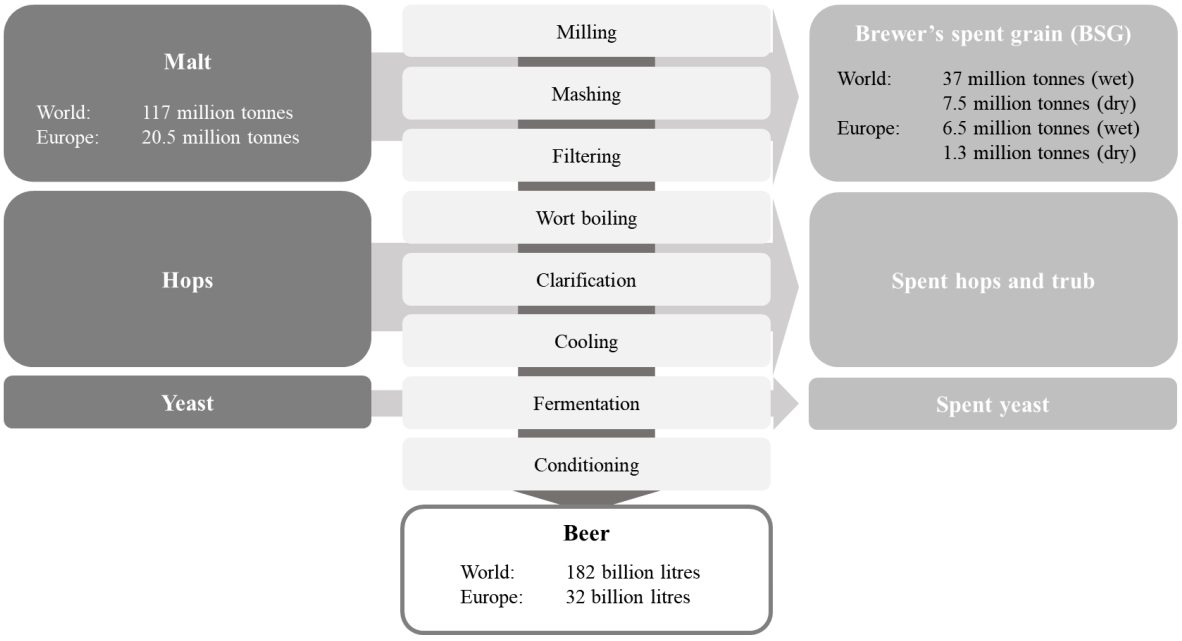

Figure 1. Schematic representation of the industrial brewery process and the by-products involved. Data for the use of feedstock, generation of wet BSG and beer production data is from 2020 [11–15].

BSG is a readily available by-product that consists of the barley grain husks together with parts of the pericarp and seed coat layer that is obtained as solid residue after the production of beer wort. Even if progress in technologies has permitted improvements in the process, in terms of quantity of by-products and efficiency, the quantity of residual BSG is difficult to

reduce. In terms of BSGs generation, considering the global manufacture of beer in 2020 of 182 billion litres [11], of which around 32 billion litres were produced in Europe [12], a global amount of 37 million tonnes of wet BSG is estimated (7.5 million tonnes on dry basis) [13–15]. BSG production yield is around 20 kg of wet BSG per 100 L of brewed beer, and the wet BSG contains between 70 and 80% of water [16].

Although deposition of such residue may be a reasonable option for management, new uses of this waste may be explored from an economical perspective [17,18]. Among the different alternatives, involving the production of activated carbon, biomethane production, extraction of high-value compounds from BSG, animal or human nutrition, or fertilisers, energetic valorisation stands out as a promising environmental option [19–21]. Even if this biomass presents a suitable composition for energy valorisation processes, they are usually wet and involve a significant obstacle for being used as a solid biofuel and, therefore, a drying stage is required to moisture content lower than 15% [22]. Moreover, they have morphological heterogeneity, and thus, a study of their decomposition kinetics during thermochemical conversion becomes essential to understand their degradation mechanism before its use as energy vectors [23].

The evaluation of the decomposition kinetics has been widely applied for developing a model for the energy valorisation of biomass in full-scale systems [24,25]. Most studies in the literature are related to the kinetics of biomass decomposition during pyrolysis under inert atmospheres [26–28]. However, the evaluation of the oxidative decomposition for the simulation of combustion reactions has been scarcely explored, especially in BSGs. Reactions underwent in the oxidative atmosphere are usually heterogeneous and complex and commonly result in the generation of intermediate species due to both synergistic pyrolytic and oxidation phenomena [29,30]. According to the literature, gasification is recognized as the best technique for thermochemical conversions of biomass [31]. Different reactor

configurations could be used for this purpose, such as fixed bed reactors, fluidized bed reactors, or spouted bed reactors among others [32]. For a suitable implementation of biomass in the industrial-scale application, a deep understanding of the oxidative kinetics when submitted to high temperature is necessary to find the best operational conditions in terms of design, scale-up, and feasibility [3].

A useful method for the evaluation of parameters for the design and optimization of the valorisation setup can be obtained using thermogravimetric analysis (TGA) when non-isothermal multiple heating rates are applied [33]. From these analyses, the main kinetic parameters can be calculated and serve as the baseline for the energy valorisation of BSGs in large-scale gasification processes that allow for product yield control [34,35]. For this purpose, a combination of iso-conversional methods, along with the use of Master-Plots and the use of the Perez-Maqueda *et al*. criterion permitted to assess the so-called kinetic triplet of BSGs: activation energy (*Ea*), the pre-exponential factor (*A*), and the kinetic function *f(α)*. Finally, the feasibility of BSGs for being used as fuels in a pilot spouted bed reactor was verified.

2. Materials and methods

2.1. Materials and sample preparation

Brewer's spent grains (BSG) of pure Carafa, Aroma, Crystal, Pale Ale, Trigo, and Pilsener malt varieties were purchased from *Tu Cerveza Casera Homebrew* and processed in a 20 L pilot-scale brewing installation. Firstly, the malt was crushed in a mill. Then the boiler was filled with water and heated up to 65 ºC with a heating rate of 1 °C·min^{-1}. Then, the mashed malt was added and thoroughly mixed, so that the malt mass was obtained, and allowed for fermentation for 1 h. During the fermentation process, the pH was kept at 5.50 with the aid of a few mL of lactic acid. Finally, the temperature was increased up to 75 °C for 5 min, before

filtering and rinsing. For filtering, a Brewferm filter bowl was used, equipped with a perforated filter plate and a tap. At this point, the malt mass was rinsed with water at 78 °C. Afterwards, rinsed malt mass was pressed to remove water and subsequently dried at 50 ºC on a large surface until a constant mass was reached, approximately 48 h. Lastly, BSGs were ground using a Moulinex Super Junior "S" grinder, and the obtained powders were conserved in a desiccator. The microscopic appearance of the powders was evaluated using a Leica MZ APO system.

2.2. Proximate analysis

Ash (*A*), volatile matter (*VM*), and moisture (*M*) contents of the BSGs were measured according to the standardized procedures described in ISO 18122:2016 (Solid Biofuels – Determination of ash content) [36], ISO 18123:2016 (Solid biofuels – Determination of the content of volatile matter) [37], and ISO 18134-1:2016 (Solid biofuels – Determination of moisture content – Oven dry method – Part 1: Total moisture – Reference method) [38], respectively. The fixed carbon (FC) was determined by the difference of these values, according to **Equation 1**.

$$FC(\%) = 100 - M\ (\%) - VM\ (\%) - A\ (\%) \qquad \textbf{(1)}$$

Moisture content was determined in a Heraeus Vacutherm oven while volatile matter and ashes were determined in a Thermo Heraeus M-104 muffle furnace.

2.3. Ultimate analysis

The ultimate analysis of BSGs in terms of Carbon (C), Hydrogen (H), Nitrogen (N), Sulphur (S), and Oxygen (O) was determined using a CHNS-O Thermo Flash 2000 elementary analyser, operating at 900 °C in an atmosphere of pure oxygen. The oxygen content was calculated by the difference on a dry and ash-free basis according to **Equation 2**.

$$O(\%) = 100 - C(\%) - H(\%) - N(\%) - S(\%) \quad \textbf{(2)}$$

2.4. Higher heating value

The higher heating value was calculated using the equation proposed by Channiwala and Parikh, using carbon (C), hydrogen (H), nitrogen (N), sulphur (S), oxygen (O), and ash (A) weight percentages, according to **Equation 3**.

$$HHV\ (MJ/kg) = 0.3491 \cdot C\ (\%) + 1.1783 \cdot H\ (\%) + 0.1005 \cdot S\ (\%) - 0.1034 \cdot O\ (\%) - 0.0151 \cdot N\ (\%) - 0.0211 \cdot A\ (\%) \quad \textbf{(3)}$$

2.5. Thermogravimetric analysis (TGA)

The thermogravimetric analysis (TGA) was carried out with a Mettler Toledo TGA/STDA 851^e setup. The samples, with a mass between 2 and 5 mg, were placed in triplicates into 70 µL alumina capsules. The analyses were performed with multi-rate non-isothermal segments (β = 2, 5, 10, 20 and 30 ºC·min^{-1}) from 25 to 800 °C under an oxidative atmosphere with a flux of 50 mL·min^{-1} of pure oxygen. The obtained results were evaluated with the aid of the software STARe 9.10 from Mettler Toledo.

2.6. Kinetic analysis of the decomposition

2.6.1. Apparent activation energy

The most effective methods for the determination of the kinetic parameters are based on the analysis of dynamic thermogravimetric measurements obtained at different heating rates (β). Given that the kinetic parameters vary with the progress of the decomposition, iso-conversional methods, serve to calculate the evolution of activation energy during conversion. These methods use data from different multi-linear non-isothermal experiments

and avoid model assumptions for the analysis, which are the main source of error of model-fitting methods. In this study, multiple-α integral methods proposed by Flynn-Wall-Ozawa (FWO) and Kissinger-Akahira-Sunose (KAS) along with differential method given by Friedman were considered.

Flynn, Wall and Ozawa proposed the solution described in **Equation 4**, assuming the Doyle approximation, based on the Schlömilch expansion. The activation energy for different conversions can be calculated from the slope of the plots of log β versus the reciprocal of temperature.

$$\log\beta = \log\frac{Ea \cdot A}{R \cdot g(\alpha)} - 2.315 - \frac{0.457 \cdot Ea}{R \cdot T} \quad (4)$$

Kissinger-Akahira-Sunose (KAS) proposed a similar approach, by following **Equation 5**, where *g(α)* is the inverse integral kinetic model $g(\alpha) = \int_0^\alpha \left(f(\alpha)\right)^{-1} d\alpha$. The activation energy may be taken from the slope of ln (β/T^2) versus the reciprocal of temperature.

$$\ln\left(\frac{\beta}{T^2}\right) = \ln\left(\frac{A \cdot R}{Ea \cdot g(\alpha)}\right) - \frac{Ea}{R} \cdot \frac{1}{T} \quad (5)$$

Friedman proposed **Equation 6**, in which the activation energy at a specific conversion degree can be obtained from the slope of ln (dα/dt) versus the reciprocal of temperature.

$$\ln\left(\frac{d\alpha}{dt}\right) = \ln(A \cdot f(\alpha)) - \frac{Ea}{R} \cdot \frac{1}{T} \quad (6)$$

2.6.2. Analysis of the kinetic function

Thermal and thermo-oxidative decompositions in full-scale systems are described in terms of intrinsic kinetics, in which heat and mass transfer limitations are not included. These models circumvent the rigorous and exhaustive description of the chemistry of thermal

decomposition and describe the process using a simplified reaction pathway. It is widely known that each single reaction step is representative of a complex network of reactions. Among the different solid-state mechanisms, a sigmoidal function or a deceleration function are frequently selected to describe the kinetic mechanism.

Master Plots (MP) involve referencing theoretical curves depending on the kinetic model, which is generally independent of the kinetic parameters of the process. In many cases, the experimental kinetic data can easily be transformed into experimental curves and the comparison with the MPs allows for the selection of the appropriate kinetic model of the process under investigation. In this study, MPs were based on the integral form of the generalized kinetic equation (MP_g), reduced at $\alpha = 0.5$ for better visualization, as described by Criado [39]. This method also allows the determination of the kinetic model, when the activation energy is already known [39]. The kinetic analysis of the non-isothermal process is normally carried out employing a single-step kinetic equation (**Equation 7**), which integration leads to the inverse integral kinetic function *g(α)*, as shown in **Equation 8**.

$$\frac{d\alpha}{dt} \equiv \beta \cdot \frac{d\alpha}{dT} = A \cdot f(\alpha) \cdot k(T) = A \cdot f(\alpha) \cdot e^{\frac{Ea}{R \cdot T}} \quad (7)$$

$$g(\alpha) = \int_0^{\alpha} \frac{d\alpha}{f(\alpha)} = \frac{A \cdot Ea}{\beta \cdot R} \cdot \int_0^{\infty} \frac{e^{-x}}{x^2} = \frac{A \cdot Ea}{R \cdot T} \cdot p(x) \quad (8)$$

where $x = \frac{E}{R \cdot T}$ and $p(x) = \frac{e^{-x}}{x^2} \cdot \sum_n \frac{n \cdot (1-n)}{x+2 \cdot (n+1)}$ is the result of the Senum and Yang approximation. The Senum and Yang's approximation was truncated at the fifth term since it permits obtaining a good approximation for a given temperature integral for $x > 10$ [40].

Once were evaluated the activation energies, the calculated *g(α)* were compared with the master plots and the mechanism was ascertained.

2.6.3. Pre-exponential factor and reaction order calculation

The kinetic triplet was completed with the pre-exponential factor (*A*) and reaction order (*n*). For this purpose, the Perez-Maqueda *et al.* criterion (*P-Mc*) was applied. This criterion relies on the independence of the activation energy (*Ea*) and the pre-exponential factor (*A*) on the heating rate (β), which must be assessed with the aid of the Coats-Redfern expression shown in **Equation 9**.

$$\ln\frac{\beta \cdot g(\alpha)}{T^2} = \ln\frac{A \cdot R}{Ea} + \frac{Ea}{R} \cdot \frac{1}{T} \qquad (\mathbf{9})$$

If so, the minimization of ξ in **Equation 10** will give the proper reaction order (*n*) for the model and, subsequently, the most precise pre-exponential factor (*A*), by averaging the values from the intercept at y = 0 of the Coast-Redfern equation.

$$\xi(n,\alpha) = \sum_{i}^{h} \left| (-R) \cdot \frac{d}{dt}\left(\frac{\ln(\beta_i \cdot T^{-2} \cdot g(\alpha))}{T^{-1}}\right) - Ea_{iso} \right| \qquad (\mathbf{10})$$

2.7. Combustion of BSGs in a pilot incineration plant

As a validation approach, the dry beer spent grains (BSGs) of the different malt varieties were pelletised together in a Smart Wood PLT-50 setup, with a production capacity of 20-30 $kg \cdot h^{-1}$. Pellets with a diameter of 6 mm and a length of 30 mm were obtained, which morphology is shown in **Figure 2**. Afterwards, they were subjected to isothermal combustion for 1 h at temperatures in the range from 400 to 700 ºC in steps of 50 ºC in a Thermo Heraeus M-104 muffle furnace, to validate the ash yields and the appearance after combustion.

Finally, 1 kg of the pelletised BSGs was applied in an own-designed pilot incineration plant, such as that shown in **Figure 2**. The setup was equipped with a hopper with a base square 0.5 m length and inclined walls together with a cylindrical bar to promote vibrations to prevent

blocks. The feeding mass flow was controlled by a rotary valve with a diameter of 4.86 cm, previously calibrated. Then, the conveyor belt with dimensions of 4.55 m length, 0.15 m wide, and spaced partitions every 0.175 m, allows for the transport of the pellets to the feeding tube regulated by a rotary valve and subsequently to the incineration unit. The incineration unit consists of a combustion chamber with a moving grill in a circular motion to prevent potential slagging. Inside this chamber, two ignition glow plugs with lengths 140 mm and 250 W each are installed, along with four temperature sensors monitor the temperature of the top, the gas outlet, the heart of the combustion chamber, and the collector of ashes. Air is conveyed from the downstream of the combustion chamber to ensure combustion and extract fumes from the chamber. Ashes are recovered into a tray located at the bottom of the chamber, with dimensions of 19×30.4×9.4 cm^3. The tightness of the chamber was ensured with an isolated door that included a viewing port. Overall, the operating conditions were feeding rate of ~1 $kg \cdot h^{-1}$ and airflow of 50 $L \cdot min^{-1}$ (21% O_2), to assure combustion temperatures above ~500 ºC during operation. Once the mentioned amount of pellet was consumed, the remnant ash was collected and the yield and apparent density were calculated.

Figure 2. Pellets of dry brewer's spent grains (BSG), an overview of the pilot incineration plant and detail of the incineration unit.

3. Results and discussion

3.1. Initial characterization of the biomass

The brewer's spent grains (BSG) of pure Carafa, Aroma, Crystal, Pale Ale, Trigo, and Pilsener malt varieties were initially characterised. For this purpose, the macroscopic appearance, the microscopic morphology, and the composition −both by proximate and ultimate analyses− were evaluated and the obtained results are shown in **Table 1**.

In terms of macroscopic appearance, milled and dried BSGs revealed different colours, which are due to the particular malt variety and preparation conditions [41]. These colours are strictly correlated to the flavours that malt brings to the beer [42]. Indeed, malt flavours are used to bring balance to beer and are the source of limitless combinations for differentiation [43]. Dark roasted grains such as those of Carafa are used to impart a signature rustiness reminiscent of coffee or chocolate and contribute to significant levels of colour to beer. However, they are frequently used in lower percentages below 5% to avoid intense modifications. Typically, these roasted malts infer a beer colour of 800 to 1000 EBC (European Brewing Convention). Conversely, amber malts such as the Aroma variety, bring hints of toasted walnut, dark caramel, and dried fruit with a colour of 350 to 450 EBC and can be used in percentages up to 15%. Then, the Crystal, Pale Ale, Trigo or Pilsener malts can bring smother flavours and colours varying from 100 to 400 EBC, according to the stewing phase and the pre-roasting temperatures.

The microscopic morphology of the powder after grinding revealed a relatively homogeneous structure, with the size of grain lower than 1 mm. The preparation of uniform powder samples is crucial for a representative evaluation of the biomass, especially in terms of homogeneity during further thermo-oxidative stability and kinetic analysis of decomposition.

Subsequently, the moisture (*M*), volatile matter (*VM*), fixed carbon (*FC*), and ash (*A*) along with the weight proportion of the constituting elements (C, H, O, N and S) were evaluated to validate BSGs as solid biofuels [44]. Overall, the proximate analysis showed similar percentages of moisture, volatiles, ash yield, and fixed carbon for all the BSGs regardless of the malt variety. The applied drying procedure permitted to obtain a very low retained moisture percentage, below 1.5%. Volatile content was comparable among all the BSGs and ranged between 86 and 95%. The perceived differences may be ascribed to the remnant presence of low molar mass molecules such as extractives or polysaccharides from the maceration stage. Ash yield was around 2% in all the BSGs except in the Carafa malt variety, in which it was significantly higher, reaching 5.4%. The specific roasting treatment of this malt before maceration may be responsible for this high ash yield.

In terms of ultimate analysis, Carbon, Hydrogen, Oxygen, and Nitrogen percentages were virtually equal in the BSGs of all the malt varieties. A close view of the obtained values highlights the higher Carbon percentage for Carafa's BSGs. Again, the different roasting nature of this malt would be responsible for this behaviour. This higher percentage of C implies a higher calorific value and, from the point of view of energy production, it enhances its suitability in thermo-chemical conversion processes. A null content of Sulphur and low Nitrogen content was found for all analysed BSGs, which suggests the improbable production of unwanted SO_x and NO_x compounds during combustion.

Finally, the higher heating value was calculated applying the equation of Channiwala and Parikh [45], and values between 17.8 and 19.1 $MJ \cdot kg^{-1}$ were achieved, higher than those described for agri-food and agricultural residues, with reported HHVs around 15 $MJ \cdot kg^{-1}$ [8,24,25]. This observation together with the null Sulphur content and the low percentages of ash yield, approve these materials for the production of bioenergy.

Table 1. Macroscopic appearance of the milled and ground dry BSGs and microscopic images of the obtained powders. Scale bar in micrographs represents 1 mm.

		Carafa	Aroma	Crystal	Pale Ale	Trigo	Pilsener
Macroscopic appearance of the milled BSGs							
Macroscopic appearance of the ground BSGs							
Microscopic morphology of the powders		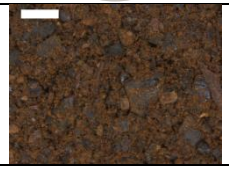	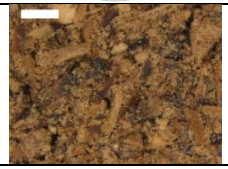	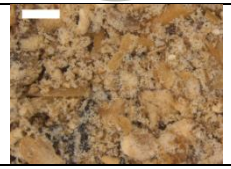	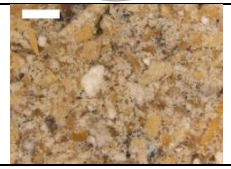	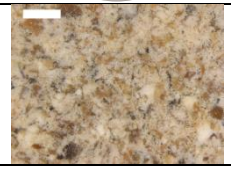	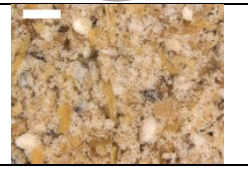
Proximate analysis (% w/w)	**Moisture (*M*)**	0.7	0.6	1.2	0.4	0.8	1.1
	Volatile matter (*VM*) [c]	88.3	91.8	86.6	95.3	95.6	92.2
	Fixed carbon (*FC*) [a,c]	5.5	5.9	10.4	2.0	1.2	4.6
	Ash (*A*)[c]	5.4	1.7	1.7	2.3	2.5	2.1
Ultimate analysis (% w/w)	**C**[b]	46.7	44.7	44.4	44.6	44.4	44.0
	H[b]	6.4	6.4	6.4	6.6	6.6	6.4
	N[b]	44.3	47.3	47.8	46.9	46.9	48.2
	S[b]	2.6	1.6	1.4	1.9	2.1	1.4
	O[a]	-	-	-	-	-	-
***HHV* (MJ·kg^{-1})**		19.1	18.2	18.1	18.4	18.3	17.8

([a])Obtained by difference; ([b])Weight percentage on dry ash-free basis; ([c])Weight percentage on dry basis.

3.2. Thermo-oxidative stability

The thermo-oxidative stability of the BSGs was assessed at different heating rates (β = 2, 5, 10, 20 and 30 ºC·min^{-1}) and the thermogravimetric (TG) and first derivative curves (DTG) were obtained. For demonstration purposes, **Figure 3** shows the TG and DTG curves for the BSGs analysed at β = 10 ºC·min^{-1}. The TG and DTG curves were furtherly analysed, and the onset and endset decomposition temperatures (T_o, T_e), the peak temperature (T_p), and the mass loss percentages for the different stages (Δm) were calculated for this heating rate, which values are gathered in **Table 2**.

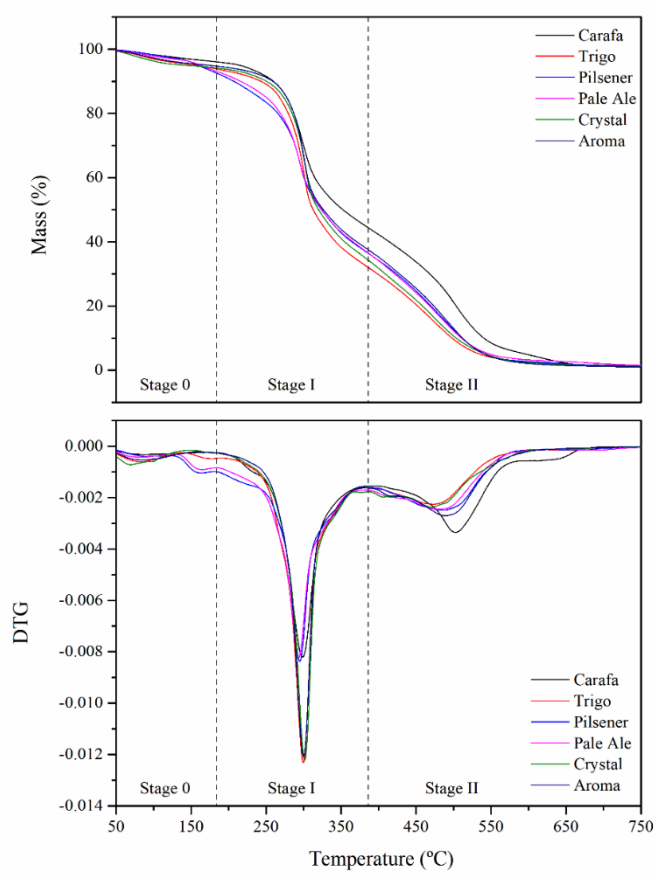

Figure 3. Thermogravimetric (TG) and first derivative (DTG) curves of the dry BSGs measured at β = 10 ºC·min^{-1}.

Table 2. Onset and endset decomposition temperatures (T_o, T_e), peak temperature (T_p) and mass loss percentages for the different thermo-oxidative degradation stages (Δm) obtained at β = 10 ºC·min^{-1} for the dry BSGs. A standard deviation below 2% was omitted for the sake of clarity.

	Onset	**Stage 0 (Humidity + volatiles)**		**Stage I (Cellulose + hemicellulose + lignin)**		**Stage II (Lignin + char)**		**Endset**	***Δm_1/ (Δm_2- 25%*)***
	***T_o* (ºC)**	***T_{p0}* (ºC)**	***Δm_0* (%)**	***T_{p1}* (ºC)**	***Δm_1* (%)**	***T_{p2}* (ºC)**	***Δm_2* (%)**	***T_e* (ºC)**	
Carafa	265.1	91.1	3.2	298.7	56.1	505.6	42.5	547.1	3.2
Aroma	274.8	86.2	4.3	300.3	60.6	491.6	38.5	533.5	4.5
Crystal	275.4	77.4	5.1	300.0	61.8	476.9	37.0	529.6	5.2
Pale Ale	264.7	91.1	3.6	293.9	62.2	481.0	37.7	527.8	4.9
Trigo	273.0	82.2	4.5	298.6	66.5	472.7	32.5	523.3	9.0
Pilsener	258.6	96.0	2.8	294.1	61.3	483.9	37.5	537.2	4.9

*According to char content reported in [46].

The initial mass loss with a percentage below ~5% occurred from 25 to 170 °C with a peak (T_{p0}) located between 80 and 90 ºC. This stage is mainly due to water vaporization but also caused by proteins and extractives decomposition, especially above 150 ºC perceivable for BSGs from Pilsener, Pale Ale and Trigo malts.

Afterwards, two main decomposition stages were found, according to expectations for lignocellulosic biomass [34]. Stage I involved the decomposition between 170 and 380 ºC and Stage II from 380 ºC onwards. Although this two-stage behaviour has been widely reported in the literature, different approaches have been proposed for the identification of the components decomposing in each stage. It has been proved that the synergistic and simultaneous purely pyrolytic thermal degradation and heterogeneous oxidation occur during decomposition in the oxidative atmosphere, giving, as a result, a complex thermogram. Therefore, the mass loss profile during thermogravimetric analysis may be the sum of the pyrolysis of biomass, the heterogeneous oxidation reactions, and the combustion of the generated char. If the biomass composition is considered as a combination of hemicellulose, cellulose, and lignin, the peaks in the DTG curve would be assigned according to the reported

stability of these components. However, the reaction mechanism corresponding to the different peaks has been the focus of discussion and two hypotheses have been proposed. The first hypothesis describes that during Stage I, the complete volatilization of the three main constituents (hemicellulose, cellulose, and lignin) occurs, followed by the combustion of char residue in Stage II [47]. Conversely, the second hypothesis considers that in Stage I the hemicellulose and cellulose are completely degraded, while lignin is partially decomposed in Stage I and also in Stage II. Therefore, Stage II would involve the completion of the volatilisation of the lignin together with the decomposition of the char. This second hypothesis has been recently proved by Ding *et al.*, demonstrating that the decomposition of lignin is a long-lasting process that contributes to both Stages I and II [34].

In the current study, the decomposition of hemicellulose, cellulose, and partial lignin was intuited during Stage I. Subsequently, lignin and char volatilization were supposed from 380 ºC onwards during Stage II. This behaviour was validated through the evaluation of the mass loss for both stages. Coronado *et al.* studied the composition of brewer's spent grains (BSGs) in terms of hemicellulose, cellulose, and lignin and compared their results with those previously reported in the literature [48]. If their reported percentages are averaged, the general composition of the BSGs would result as 28.4% (±5.3%) hemicellulose, 20.6% (±3.4%) cellulose, and 13.6% (±1.9%) lignin. This composition would be equivalent to proportions of hemicellulose+cellulose to lignin close to 3.5/1. Considering the char yield for BSGs in purely pyrolytic processes of around 25% [46], Stage II in this study would involve between 7.5 and 17.5% of lignin decomposition contribution. Therefore, the proportion of the mass loss percentage for Stage I versus the remnant lignin in Stage II, *i.e.* $\Delta m_1/(\Delta m_2\text{-}25\%)$ shown in **Table 2**, corroborates that the decomposition of lignin started during Stage I and was completed during Stage II, demonstrating the second proposed hypothesis.

In terms of onset temperature (T_o), non-significant differences were found, and it can only be highlighted the lowest onset temperature for the Pilsener's BSGs, which started substantial mass-loss from 258 °C onwards. The peak temperatures of the main decomposition stage (T_{p1}) remained unaltered and mass loss contributions were quite similar for all the varieties. The only difference to be noted was in the Carafa's BSGs, in which the mass loss was a little lower than the average and the temperature of the peak was higher than that of all the other BSGs. Given that hemicellulose and cellulose are decomposed in this stage, it may be supposed a lower percentage of these components in such BSGs. In Stage II, non-significant changes among the analysed varieties could be identified, again except for the BSGs of Carafa malt. The peak temperature was relatively higher than the other malts and the mass loss in this stage was also bigger, suggesting a greater char production during combustion. This observation was also confirmed by the highest ash yield and lower volatiles content obtained in the proximate analysis section. The shift to higher temperatures of the Carafa's BSGs was also visible in the endset temperature (T_e).

At this point, the contribution of the heating rate to the thermo-oxidative stability of the BSGs was evaluated. As an illustrating representation, the thermogravimetric (TG) and derivative thermogravimetric curves (DTG) for Carafa's BSGs as a function of the heating rate are shown in **Figure 4**. Results for the other BSGs with an analogous pattern are shown in **Figures S1** and **S2** in the Supplementary Material. According to expectations, higher heating rates displaced both decomposition processes (Stage I and Stage II) towards higher temperatures during thermo-oxidative decomposition for all the BSGs regardless of the malt variety. Heat transfer during faster heating may be limited, and therefore, higher peak temperatures were found [25,49]. To avoid the influence of the dynamic heating program during thermogravimetric analyses, the thermo-oxidative decomposition behaviour (*TDB*)

when the heating rate tends to zero *(β→0)* was calculated, adjusting the results to the exponential relationship shown in **Equation 11**, where *a*, *b* and *k* are parameters of the fitting.

$$TDB(\beta) = \frac{a}{1 + b \cdot e^{-k \cdot \beta}} \qquad \textbf{(11)}$$

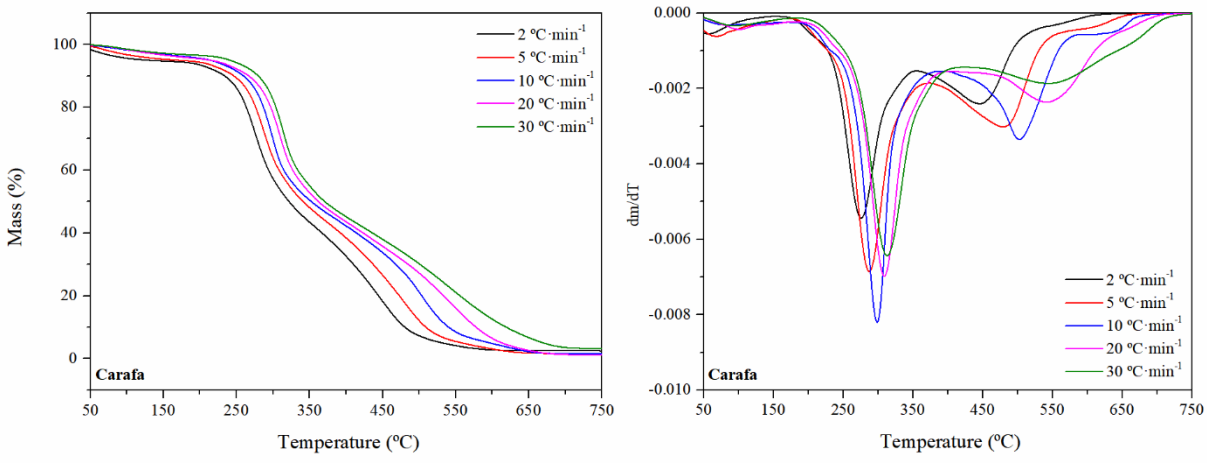

Figure 4. Thermogravimetric (TG) and first derivative (DTG) curves of Carafa's dry BSGs measured at β = 2, 5, 10, 20, and 30 ºC·min^{-1}.

In particular, the zero-decomposition temperature (*ZDT*) for the onset (T_o), Stage I (T_{p1}), Stage II (T_{p2}), and endset (T_e) temperatures were assessed. For demonstrative purposes, the fitting of the model as a function of the heating rate for Carafa's BSGs is plotted in **Figure 5**. Results for the other BSGs with analogous patterns are shown in **Figure S3** in the Supplementary Material. **Table 3** gathers the obtained values along with the fitting parameters and regression coefficient for all the BSGs. Although most of the fitting lines showed a high degree of correlation (R^2) generally above 0.95, the BSGs should be compared with caution. While all the calculated values of *ZDT* give valuable information, the technological utility of the beginning and ending of the decomposition given by the onset and endset temperatures (T_o and T_e) is of great importance. Particularly, the values of the *ZDT* for the T_o were in the range from 212 to 247 ºC and decomposition finished at *ZDT* for the T_e in

the span from 462 to 495 ºC. Therefore, it can be concluded that the decomposition occurred in a temperature span of 250 ºC regardless of the BSGs variety.

Table 3. Values of Zero Decomposition Temperatures (*ZDT*) along with the fitting parameters and regression coefficient for the thermo-oxidative decomposition of dry BSGs.

		***ZDT* (ºC)**	***a***	***b***	***k***	R^2
Carafa	T_o	232	280±4	0.21±0.02	0.12±0.03	0.962
	T_1	271	314±1	0.16±0.01	0.11±0.01	0.996
	T_2	433	550±7	0.27±0.02	0.12±0.03	0.978
	T_e	495	700±63	0.49±0.26	0.04±0.03	0.940
Aroma	T_o	243	292±1	0.20±0.01	0.12±0.01	0.997
	T_1	264	316±2	0.20±0.01	0.13±0.01	0.993
	T_2	409	528±8	0.29±0.03	0.14±0.03	0.972
	T_e	464	612±27	0.32±0.04	0.08±0.03	0.948
Crystal	T_o	247	297±1	0.20±0.00	0.10±0.00	0.998
	T_1	269	320±2	0.19±0.01	0.10±0.01	0.992
	T_2	419	541±12	0.29±0.02	0.08±0.02	0.984
	T_e	462	624±10	0.35±0.02	0.06±0.01	0.997
Pale Ale	T_o	229	274±1	0.20±0.00	0.16±0.01	0.999
	T_1	263	313±4	0.19±0.02	0.11±0.03	0.976
	T_2	410	529±12	0.29±0.04	0.13±0.05	0.939
	T_e	463	644±40	0.39±0.07	0.06±0.03	0.964
Trigo	T_o	247	289±1	0.17±0.01	0.11±0.01	0.993
	T_1	265	315±3	0.19±0.02	0.13±0.03	0.976
	T_2	422	523±20	0.24±0.04	0.09±0.05	0.920
	T_e	479	628±75	0.31±0.13	0.05±0.04	0.901
Pilsener	T_o	212	267±2	0.26±0.04	0.22±0.05	0.968
	T_1	263	310±2	0.18±0.01	0.12±0.02	0.989
	T_2	428	539±26	0.26±0.05	0.07±0.04	0.935
	T_e	467	622±29	0.33±0.05	0.07±0.03	0.967

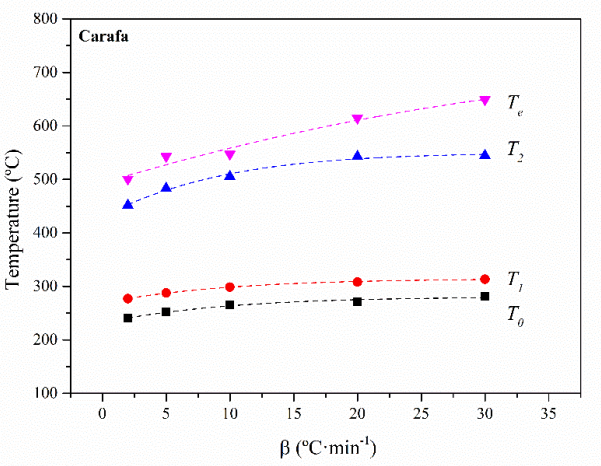

Figure 5. Evolution of the characteristic decomposition temperatures for Stages I and II (T_{p1} and T_{p2}) at all heating rates.

3.3. Kinetic analysis of the thermo-oxidative decomposition

The kinetic study of a given chemical reaction such as that of thermo-oxidative decomposition involves the (*i*) evaluation of the phenomenological kinetic laws that govern the reaction rate as a function of the concentrations of reactants and products or temperature; and (*ii*) the assessment of the mechanism of reactions (depolymerization or chain scission), or whether there is a series of stages that lead to the formation of intermediate species and products. Indeed, understanding the oxidative kinetics of biomass is essential for modelling and developing appropriate combustion methods. Although most of the approaches for the kinetic analysis proposed in the literature do not consider heat and mass transfer limitations and circumvent an exhaustive description of chemical reactions during decomposition, they offer a simplified reaction pathway valuable for the design of energy valorisation setups. In this regard, the theoretical decomposition mechanisms and their mathematical models are correlated by the kinetic functions.

The solid-state decomposition kinetics involves the calculation of activation energy (*Ea*), the pre-exponential factor (*A*), and the kinetic function *f(α)* evaluation, conforming to the so-called kinetic triplet. For this purpose, iso-conversional methods, Master-Plots, and Perez-

Maqueda *et al*. criterion were applied. In this regard, dynamic thermogravimetric analyses at different heating rates (2, 5, 10, 20, and 30 °C·min^{-1}) were considered.

3.3.1. Apparent activation energy

The apparent activation energy (*Ea*) was calculated using iso-conversional model-free approaches considering integral multiple-α methods, as described by Kissinger-Akahira-Sunose (KAS) and Flynn-Wall-Ozawa (FWO), and differential multiple-α models as the one proposed by Friedman. These methods were used for the calculation of the apparent activation energy as a function of the conversion degree (α) for the previously defined and main decomposition processes, *i.e.* Stage I (170-380 ºC) and Stage II (380-700 ºC). As an example, **Figure 6** shows the application of the FWO, KAS, and Friedman methods to the BSGs of the Carafa malt variety. All the fitting lines showed a high degree of correlation (R^2), especially for α in the range 0.2-0.6, where initiation and termination reactions are omitted. The results for the other BSGs with a comparable performance are shown in **Figures S4** and **S5** in the Supplementary Material for Stage I and Stage II, respectively.

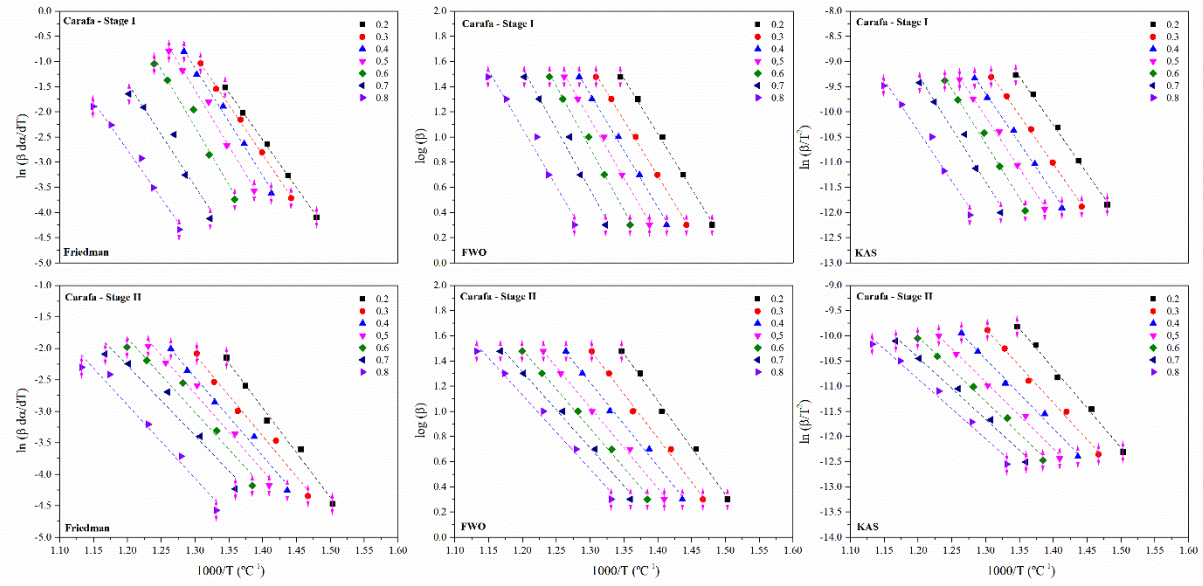

Figure 6. Application of the Friedman, FWO, and KAS and methods to the decomposition during Stage I and II for the Carafa's dry BSGs.

The obtained apparent activation energy (*Ea*) for the BSGs of all the malt varieties are shown in **Figure 7** as a function of the conversion degree, calculated as an average of the results obtained by the Friedan, FWO, and KAS methods. Moreover, the *Ea* was furtherly averaged in the α range from 0.2 to 0.8 and the obtained values are gathered in **Table 4** for the Stages I and II, separately. The apparent activation energy was fairly similar for the FWO and KAS methods, while were to some extent different for the Friedman method, also with higher average deviation. This could be due to the differential nature of this method that, after the required numerical differentiation, could give this slightly diverse result [25]. Overall, results were in line with other studies dealing with different types of lignocellulosic biomasses, in which activation energy is reported in the range 140-200 kJ·mol^{-1} for the given α range [50,51].

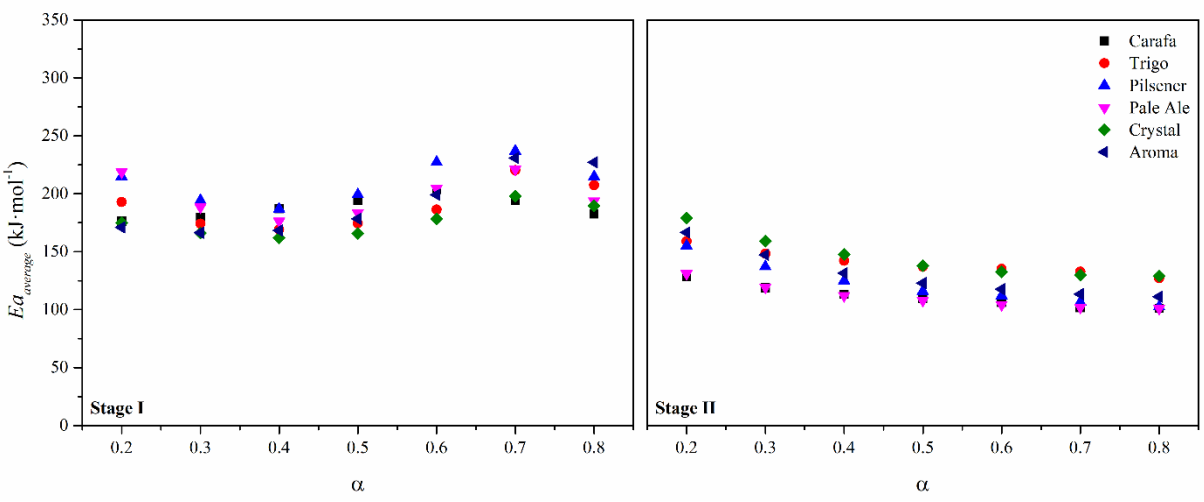

Figure 7. Average of the apparent activation energy (*Ea*) as a function of the conversion degree calculated through Flynn-Wall-Ozawa (FWO), Kissinger-Akahira-Sunose (KAS), and Friedman for all the dry BSGs during Stages I and II.

Table 4. Average of the apparent activation energy calculated in the range from α = 0.2-0.8 through Flynn-Wall-Ozawa (FWO), Kissinger-Akahira-Sunose (KAS), and Friedman for all the dry BSGs during Stages I and II.

	Stage I			**Stage II**		
	Ea_{FWO} (kJ·mol^{-1})	Ea_{KAS} (kJ·mol^{-1})	$Ea_{Friedman}$ (kJ·mol^{-1})	Ea_{FWO} (kJ·mol^{-1})	Ea_{KAS} (kJ·mol^{-1})	$Ea_{Friedman}$ (kJ·mol^{-1})
Carafa	187±7	187±7	191±12	119±8	112±9	103±6
Aroma	186±19	187±20	202±34	139±17	134±18	117±14
Crystal	176±9	176±9	178±20	153±15	148±17	135±12
Pale Ale	198±12	199±12	197±24	119±9	113±10	102±6
Trigo	188±14	189±15	191±25	147±8	142±9	133±7
Pilsener	208±13	210±13	215±20	132±15	126±16	109±13

As expected, the activation energy for Stage I was significantly higher (190-200 kJ·mol^{-1}) than that of Stage II (100-150 kJ·mol^{-1}) due to the subsequent decomposition of pure components and char, respectively. Although slight differences were found for a given stage, the calculation of the apparent activation energy after the separation of the process into two main stages was demonstrated to be suitable for such biomass, which suffers heterogeneous reactions when subjected to thermo-oxidative decomposition [52,53].

3.3.2. Evaluation of the kinetic model

The use of reduced Master Plots (MP) to ascertain the mathematical decomposition model allow for obtaining the reaction mechanism during thermo-oxidative decomposition [25,54,55]. MP offer theoretical curves which are superposed to experimental data to select the adequate kinetic model for the given reaction. The normalized $MP_{g(\alpha)/g(0.5)}$ along with the experimental curves obtained with a heating rate of 10 ºC·min^{-1} for the different BSGs during Stage I and Stage II are represented in **Figure 8**.

When MP and experimental curves were compared, it was found that all the reaction mechanisms for Stage I were comparable to curve F_n type, with n equal to 2, 3, 4, and 5.

Physically speaking, *F* mechanisms represent solid-state processes, in which random nucleation with one, two, or three nuclei on the individual particle takes place. However, Stage II revealed a mechanism more difficult to assign. Although experimental curves were always between F_n and D_n models, the mechanism selected as the most appropriate to describe all the experimental results of Stage II was the D_4 type. This mechanism was furtherly corroborated in the next section and describes a solid-state process in which three-dimensional diffusion occurs. These identified mechanisms, which algebraic expressions for $f(\alpha)$ and $g(\alpha)$ are presented in **Table 5**, are in accordance to results reported in the literature, in which the mechanism of decomposition of lignocellulosic materials under oxidative conditions for temperatures in the range of those selected for Stage I (mostly attributed to hemicellulose and cellulose) is often identified as an F_n mechanism, while the decomposition of Stage II (attributed to remaining lignin and char) is sometimes described according to F_n, A_n or D_n mechanisms for different materials [24,25,56].

Table 5. Algebraic expressions for the differential $f(\alpha)$ and integral $g(\alpha)$ functions for the selected mechanisms of the solid-state processes.

Mechanism	$f(\alpha)$	$g(\alpha)$	Solid-state process
F_1	$1-\alpha$	$-\ln(1-\alpha)$	Random nucleation with one nucleus on the individual particle
F_2	$(1-\alpha)^2$	$1/(1-\alpha)$	Random nucleation with two nuclei on the individual particle
F_3	$\frac{1}{2}(1-\alpha)^3$	$1/(1-\alpha)^2$	Random nucleation with three nuclei on the individual particle
F_4	$\frac{1}{3}(1-\alpha)^4$	$1/(1-\alpha)^3$	Random nucleation with four nuclei on the individual particle
D_4	$\frac{3}{2}[(1-\alpha)^{-\frac{1}{3}}-1]$	$\left[1-\left(\frac{2}{3}\right)\alpha\right]-(1-\alpha)^{\frac{2}{3}}$	Three-dimensional diffusion

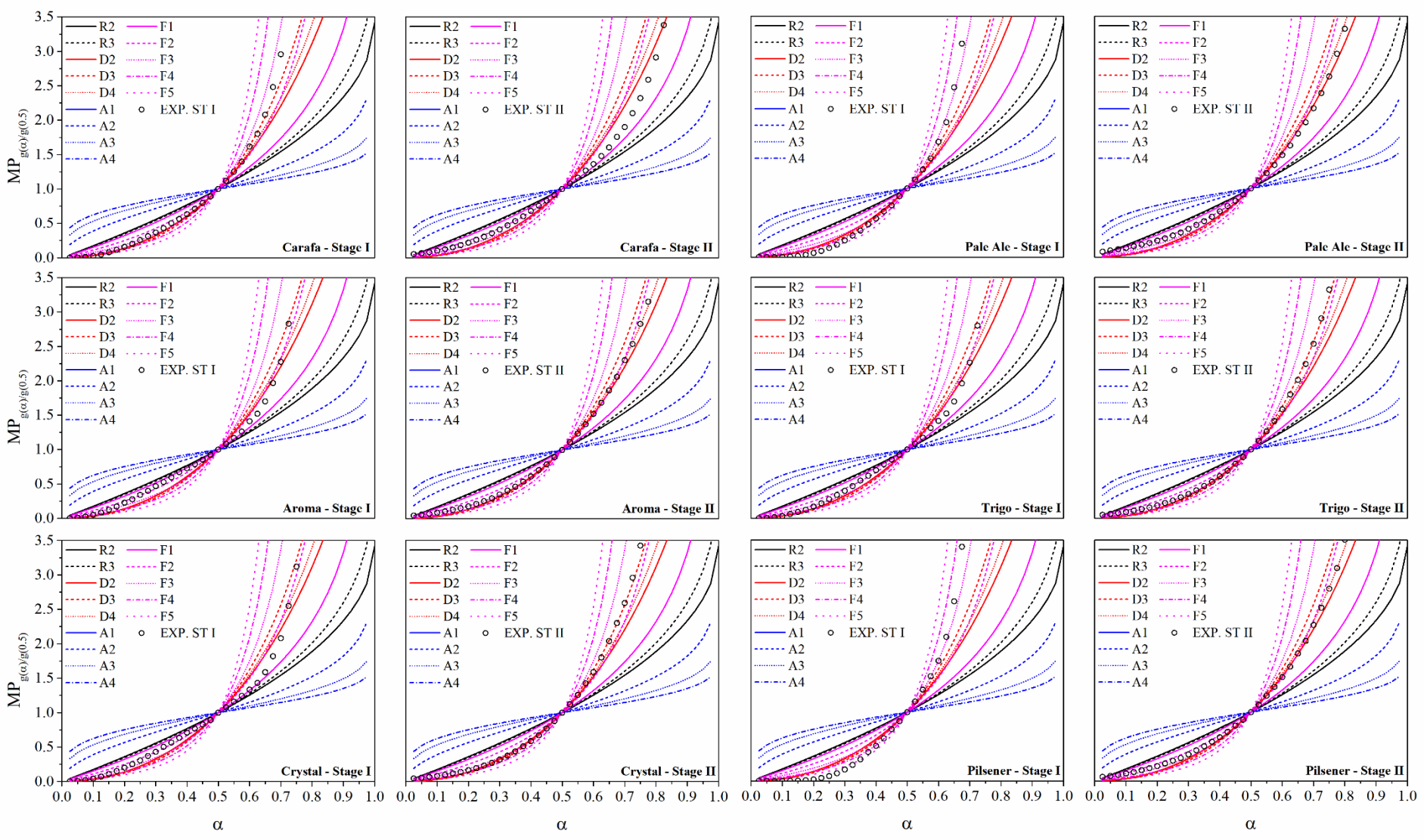

Figure 8. Comparison of the theoretical and experimental master plots (*MP*) for Stage I and Stage II of the different dry BSGs.

3.3.3. Determination of the pre-exponential factor and reaction order

Once the best theoretical mechanism was graphically evaluated, the pre-exponential factor (*A*) and the optimal analytical order of reaction (*n*) were assessed for the selected mechanism applying the Coast-Redfern equation (**Equation 9**). Using the average value calculated for the apparent activation energies and applying a regression method described in **Equation 10**, the order of reaction was obtained. Subsequently, ln *A* was gained from the intercept of plots of $\ln\left(\beta\frac{g(\alpha)}{T^2}\right)$ vs. $\frac{1}{T}$ for each heating rate. According to the Perez-Maqueda *et al.* criterion, the points should lie on the same straight line if the appropriate *g(α)* is selected. **Figure 9** illustrates these linearly coincident representations for the Carafa's BSGs in Stage I and Stage II, respectively. The Perez-Maqueda plots for the other BSGs are shown in **Figures S6** and **S7** in the Supplementary Material. The validity of the simplified kinetic triplet was therefore demonstrated, being its use advisable when the activation energy could be considered constant within a narrow confidence interval [55]. Moreover, the good fitting of the selected mechanisms (F_n and D_4) was confirmed. However, since the passages from Stage 0 to Stage I and, from Stage I to Stage II, are not always smooth due to complex initiation and termination reactions, respectively, a small deviation from linearity was noticeable at the edges. Moreover, it can be stated that the differences for a low degree of conversion during Stage I of the Pilsener and Pale Ale BSGs are explainable by the fact that at these temperatures some trace of remnant low molar mass compounds such as extractives may still be present at the beginning of this stage.

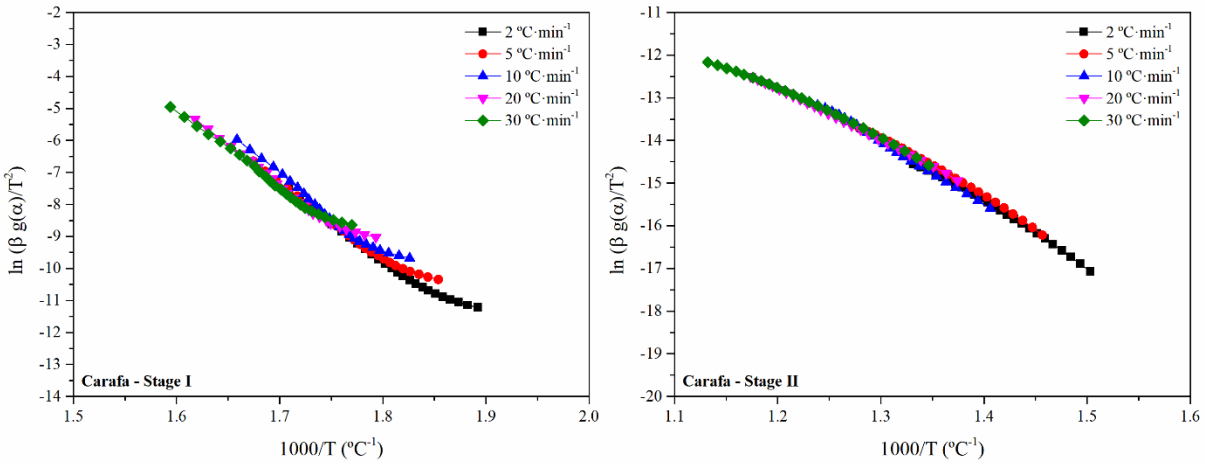

Figure 9. Application of Perez-Maqueda criterion for Carafa's dry BSGs.

Table 6 gathers the values of the Napierian logarithm of the pre-exponential factor (ln *A*) calculated from the average of the A_β at the different heating rates, the most appropriate mechanism of reaction from the Master Plots (MP), and the calculated analytical order (*n*) for all BSGs during Stage I and Stage II. Moreover, *e* (%) represents the average of absolute deviations from the mean in each set of ln A_β.

Table 6. Kinetic parameters for all the dry BSGs during thermo-oxidative decomposition in Stages I and II.

	Stage I				**Stage II**			
	ln *A*	***e* (%)**	**MP**	***n***	**ln *A***	***e* (%)**	**MP**	***n***
Carafa	40.0	6	F3	2.8	13.0	17	D4	-
Aroma	41.8	12	F2-F3	2.2	16.4	21	D4	-
Crystal	38.1	5	F2	1.9	19.1	18	D4	-
Pale Ale	40.9	7	F3	3.1	13.4	17	D4	-
Trigo	39.5	4	F2-F3	2.2	18.9	10	D4	-
Pilsener	45.6	5	F3-F4	3.7	15.3	21	D4	-

A random nucleation kinetic model (F_n) was determined for Stage I of all the BSGs, while Stage II was described by a three-dimensional diffusion kinetic model (D_4), similarly to other

lignocellulosic materials. In the order-based models, the reaction rate is proportional to the concentration of reactant raised to a particular power (integral or fractional) which is the reaction order. Conversely, in diffusion-controlled reactions, the rate of product formation decreases proportionally with the thickness of the product barrier layer [57]. Overall, the obtained results were comparable for all the analysed BSGs in the two stages, both in terms of pre-exponential factor and kinetic function, and suggest, along with the comparable calculated activation energy found in previous sections, that BSGs could be used as solid biofuels, both separately and combined, regardless of their variety or treatment.

3.4. Pelletised BSGs as combustion fuel

Given the minor perceived differences in terms of thermo-oxidative decomposition among the BSGs of the different malt varieties, the BSGs were all pelletised together. Subsequently, for validation purposes, the pellets were preliminarily subjected to isothermal combustion in a muffle furnace at different temperatures ranging from 400 to 700 ºC. These temperatures were selected according to the results found in the thermo-oxidative stability analyses, which revealed complete combustion from ~500 ºC onwards. Temperatures below 500 ºC were selected for monitoring purposes. After combustion, the ash yields were calculated and their appearance was evaluated, both gathered in **Table 7**.

O. Gil-Castell, N. Mascia, C. Primaz, F. Vásquez-Garay, M.G. Baschetti, A. Ribes-Greus. Brewer's spent grains as biofuels in combustion-based energy recovery processes: Evaluation of thermo-oxidative decomposition. Fuel, 2022; 312(122955)

Table 7. Ash percentage and appearance of the pellets of BSGs after combustion at different temperatures.

Temperature (ºC)	Ash (%)	Appearance before agitation	Appearance after agitation
400	7.05		
450	3.33		
500	3.39		
550	2.52		
600	2.64		
650	2.51		
700	2.44		

In general, ash yields below 3.5% for combustion above 450 ºC were found, which slightly decreased with higher temperatures up to 2.4% at 700 ºC. The ash percentage was comparable to that found for the combustion of the grounded BSGs measured according to normalised conditions. However, the experiments carried out at 400 ºC revealed partial combustion, with a 7.0% of residue. As a whole, the shape of the pellets remained unaltered after combustion, which turned into powder after slight agitation of the tray, especially at temperatures higher than 500 ºC. It must be highlighted that the combustion at temperatures below 500 ºC resulted in the generation of more carbonaceous ash, given the blackish colour of the powder and more consistent morphology. On the other hand, above 500 ºC, pure ash with a greyish colour was obtained, typical for the complete combustion of biomass. In this line, the combustion of BSGs in gasification processes at temperatures above 500 ºC would allow for the lowest ash yield and a powder morphology, manageable in automated setups [58] and useful for a variety of further applications [59].

This lab-scale behaviour was validated in an incineration pilot plant, in which 1 kg of BSG pellets was applied. A pellet feeding rate of ~1 $kg \cdot h^{-1}$ and airflow of 50 $L \cdot min^{-1}$ (21% O_2) were considered to ensure that combustion was accomplished at temperatures above 500 ºC. Although flames in these experimental tests experience large temporal and spatial gradients in local species and temperatures, they remained virtually constant during the whole operation, as observed through the viewing port and shown in **Figure 10** [60].

Once the pellets were consumed, the incineration unit was opened, and the remnant ash in the combustion chamber was collected into the ashtray in the bottom, as shown in **Figure 10**. The combustion ash revealed a greyish powder appearance, as found after muffle furnace combustion assays. Given the contribution of the moving grill in a circular motion of the incineration unit,

powder together with particles lower than 1.5 mm was obtained, as can be observed in **Figure 10**. For the considered amount of 1 kg of pellets, 24.12 g of ash were gained, which represents a yield of 2.4%. This result is in accordance with that found in the muffle furnace experiments at temperatures above 500 ºC, and also with that determined in the proximate analysis. Moreover, given its powder morphology, the ash revealed an apparent density of 0.37 $g \cdot mL^{-1}$. Therefore, the reliable combustion behaviour, along with the higher heating value of ~18 $MJ \cdot kg^{-1}$ found in previous sections, makes this biomass a potential candidate for being used as a source of energy in combustion incineration devices. Although ash had not adhered in the walls of the incineration unit and could be properly managed, further characterisation of ash would allow for a deeper evaluation in terms of ash formation and deposition mechanisms, particle properties or sticking behaviour [61].

Figure 10. Flame during combustion of pellets of dry BSGs (left), residue into the incineration unit after combustion (middle), and collected ash (right).

4. Conclusions

The constituting elements of the analysed beer spent grains (BSGs) are mainly Carbon and Oxygen. This, along with a low percentage of Nitrogen and a null Sulphur content makes these materials attractive for combustion purposes, providing a major environmental advantage for the

use of this biomass as a thermo-oxidation energy vector instead of fossil fuels. With an exhaustive control of the combustion temperature, the products will be mainly carbon dioxide and monoxide, while the production of unwanted nitrogenous compounds will be in non-significant proportions.

All the BSGs have similar volatiles and fixed carbon percentages, with low ash yield, that avoids operational difficulties during combustion. The acquired analogous superior higher heating value (HHV) around 18 MJ·kg^{-1} for all the BSGs highlights the benefits of using this biomass in thermo-oxidation reactions.

The global decomposition process has two main stages in the range of 212 to 495 ºC for all the BSGs. Stage I corresponds to the thermo-oxidation of hemicellulose, cellulose, and partially lignin. It follows a random nucleation kinetic model (F_n) and has a mean apparent activation energy of ~190 kJ·mol^{-1}. Stage II is related to the thermo-oxidation of and remnant lignin and char. It is described by a three-dimensional diffusion kinetic model (D_4) with a mean activation energy of ~120 kJ·mol^{-1}. These parameters can be applied as input variables in a theoretical model to describe the thermal recovery processes in a reactor using BSGs as feedstock.

The appropriate combustion process of pelletised BSGs carried out in a pilot spouted bed reactor corroborate the viability of this reaction, along with the low ash formation when combustion was carried out above 500 ºC. Overall, this BSG waste biomass may be considered a beneficial source of renewable energy in thermo-oxidation reactions, regardless of the malt variety.

Acknowledgements

The authors would like to thank the support of Generalitat Valenciana for the APOSTD/2020/155 grant for O. Gil-Castell. The Chilean Economic Development Agency (CORFO) is acknowledged for the financial support through project 13CEI2-21839 for the contract for C.T.

Primaz. The European Commission is thanked for the project LIFE-LIBERNITRATE (LIFE16 ENV/ES/000419).

Data availability

The data that support the findings of this study are available from the corresponding author upon reasonable request.

Conflict of interest

The authors declare no conflicts of interest.

References

[1] Nunes LJR, Causer TP, Ciolkosz D. Biomass for energy: A review on supply chain management models. Renew Sustain Energy Rev 2020;120:109658. doi:10.1016/j.rser.2019.109658.

[2] Balat M. An overview of the properties and applications of biomass pyrolysis oils. Energy Sources, Part A Recover Util Environ Eff 2011;33:674–89. doi:10.1080/15567030903228914.

[3] McKendry P. Energy production from biomass (part 1): Overview of biomass. Bioresour Technol 2002;83:37–46. doi:10.1016/S0960-8524(01)00118-3.

[4] Wang S, Dai G, Yang H, Luo Z. Lignocellulosic biomass pyrolysis mechanism: A state-of-the-art review. Prog Energy Combust Sci 2017;62:33–86. doi:10.1016/j.pecs.2017.05.004.

[5] Jiménez-Castro MP, Buller LS, Sganzerla WG, Forster-Carneiro T. Bioenergy production from orange industrial waste: a case study. Biofuels, Bioprod Biorefining 2020;14:1239–53. doi:10.1002/BBB.2128.

[6] Zahraee SM, Shiwakoti N, Stasinopoulos P. Biomass supply chain environmental and socio-economic analysis: 40-Years comprehensive review of methods, decision issues, sustainability challenges, and the way forward. Biomass and Bioenergy 2020;142:105777. doi:10.1016/J.BIOMBIOE.2020.105777.

[7] Zhang L, Xu C (Charles), Champagne P. Overview of recent advances in thermo-chemical conversion of biomass. Energy Convers Manag 2010;51:969–82. doi:10.1016/j.enconman.2009.11.038.

[8] Lim JS, Abdul Manan Z, Wan Alwi SR, Hashim H. A review on utilisation of biomass from rice industry as a source of renewable energy. Renew Sustain Energy Rev 2012;16:3084–94. doi:10.1016/j.rser.2012.02.051.

[9] Fatih Demirbas M, Balat M, Balat H. Biowastes-to-biofuels. Energy Convers Manag 2011;52:1815–28. doi:10.1016/j.enconman.2010.10.041.

[10] Ortiz I, Torreiro Y, Molina G, Maroño M, Sánchez JM. A Feasible Application of Circular Economy: Spent Grain Energy Recovery in the Beer Industry. Waste and Biomass Valorization 2019;10:3809–19. doi:10.1007/s12649-019-00677-y.

[11] Barth SJ, Meier H. BarthHaas REPORT Hops 2020/2021. Nuremberg: 2021.

[12] European Comission. Happy International Beer Day! - Products Eurostat News 2021. https://ec.europa.eu/eurostat/web/products-eurostat-news/-/edn-20210805-1 (accessed July 14, 2021).

[13] Mussatto SI, Dragone G, Roberto IC. Brewers' spent grain: Generation, characteristics and potential applications. J Cereal Sci 2006;43:1–14. doi:10.1016/j.jcs.2005.06.001.

[14] Mussatto SI. Brewer's spent grain: A valuable feedstock for industrial applications. J Sci Food Agric 2014;94:1264–75. doi:10.1002/JSFA.6486.

[15] Lynch KM, Steffen EJ, Arendt EK. Brewers' spent grain: a review with an emphasis on food and health. J Inst Brew 2016;122:553–68. doi:10.1002/JIB.363.

[16] Kunze W. Technology Brewing and Malting. 6th ed. Berlin: VLB Berlin; 2019.

[17] Kavalopoulos M, Stoumpou V, Christofi A, Mai S, Barampouti EM, Moustakas K, et al. Sustainable valorisation pathways mitigating environmental pollution from brewers' spent grains.

Environ Pollut 2021;270:116069. doi:10.1016/j.envpol.2020.116069.

[18] Bolwig S, Mark MS, Happel MK, Brekke A. Beyond animal feed?: The valorisation of brewers' spent grain. From Waste to Value Valoris. Pathways Org. Waste Streams Circ. Bioeconomies, Abingdon, Oxon: Routledge; 2019, p. 107–26. doi:10.4324/9780429460289-6.

[19] Nigam PS. An overview: Recycling of solid barley waste generated as a by-product in distillery and brewery. Waste Manag 2017;62:255–61. doi:10.1016/j.wasman.2017.02.018.

[20] Siqueiros E, Lamidi RO, Pathare PB, Wang Y, Roskilly AP. Energy Recovery from Brewery Waste: experimental and modelling perspectives. Energy Procedia 2019;161:24–31. doi:10.1016/j.egypro.2019.02.054.

[21] Jackowski M, Niedźwiecki Ł, Jagiełło K, Uchańska O, Trusek A. Brewer's Spent Grains—Valuable Beer Industry By-Product. Biomol 2020, Vol 10, Page 1669 2020;10:1669. doi:10.3390/BIOM10121669.

[22] Sperandio G, Amoriello T, Carbone K, Fedrizzi M, Monteleone A, Tarangioli S, et al. Increasing the value of spent grain from craft microbreweries for energy purposes. Chem Eng Trans 2017;58:487–92. doi:10.3303/CET1758082.

[23] Aliyu S, Bala M. Brewer's spent grain: a review of its potentials and applications. African J Biotechnol 2011;10:324–31.

[24] Moliner C, Aguilar K, Bosio B, Arato E, Ribes A. Thermo-oxidative characterisation of the residues from persimmon harvest for its use in energy recovery processes. Fuel Process Technol 2016;152:421–9. doi:10.1016/j.fuproc.2016.07.008.

[25] Moliner C, Bosio B, Arato E, Ribes A. Thermal and thermo-oxidative characterisation of rice straw for its use in energy valorisation processes. Fuel 2016;180:71–9. doi:10.1016/j.fuel.2016.04.021.

[26] Kaur R, Gera P, Jha MK, Bhaskar T. Pyrolysis kinetics and thermodynamic parameters of castor (Ricinus communis) residue using thermogravimetric analysis. Bioresour Technol 2018;250:422–

8. doi:10.1016/j.biortech.2017.11.077.

[27] Mishra RK, Mohanty K. Pyrolysis kinetics and thermal behavior of waste sawdust biomass using thermogravimetric analysis. Bioresour Technol 2018;251:63–74.

[28] Chong CT, Mong GR, Ng J-H, Chong WWF, Ani FN, Lam SS, et al. Pyrolysis characteristics and kinetic studies of horse manure using thermogravimetric analysis. Energy Convers Manag 2019;180:1260–7.

[29] Badia JD, Santonja-Blasco L, Martínez-Felipe A, Ribes-Greus A. A methodology to assess the energetic valorization of bio-based polymers from the packaging industry: pyrolysis of reprocessed polylactide. Bioresour Technol 2012;111:468–75. doi:10.1016/j.biortech.2012.02.013.

[30] Dhahak A, Bounaceur R, Le Dreff-Lorimier C, Schmidt G, Trouve G, Battin-Leclerc F. Development of a detailed kinetic model for the combustion of biomass. Fuel 2019;242:756–74. doi:10.1016/J.FUEL.2019.01.093.

[31] Tanger P, Field JL, Jahn CE, DeFoort MW, Leach JE. Biomass for thermochemical conversion: Targets and challenges. Front Plant Sci 2013;4. doi:10.3389/fpls.2013.00218.

[32] Epstein N, Grace JR. Spouted and spout-fluid beds : fundamentals and applications. Cambridge University Press; 2011.

[33] White JE, Catallo WJ, Legendre BL. Biomass pyrolysis kinetics: A comparative critical review with relevant agricultural residue case studies. J Anal Appl Pyrolysis 2011;91:1–33. doi:10.1016/j.jaap.2011.01.004.

[34] Ding Y, Huang B, Wu C, He Q, Lu K. Kinetic model and parameters study of lignocellulosic biomass oxidative pyrolysis. Energy 2019;181:11–7. doi:10.1016/j.energy.2019.05.148.

[35] Ding Y, Ezekoye OA, Zhang J, Wang C, Lu S. The effect of chemical reaction kinetic parameters on the bench-scale pyrolysis of lignocellulosic biomass. Fuel 2018;232:147–53. doi:10.1016/J.FUEL.2018.05.140.

[36] International Organization for Standardization. UNE-EN ISO 18122:2016 Solid biofuels. Determination of ash content. 2016.

[37] International Organization for Standardization. UNE-EN ISO 18123:2016 Solid biofuels. Determination of the content of volatile matter. 2016.

[38] International Organization for Standardization. UNE-EN ISO 18134-1:2016 Solid biofuels. Determination of moisture content - Oven dry method - Part 1: Total moisture - Reference method. 2016.

[39] Criado JM, Málek J, Ortega A. Applicability of the master plots in kinetic analysis of non-isothermal data. Thermochim Acta 1989;147:377–85. doi:10.1016/0040-6031(89)85192-5.

[40] Pérez-Maqueda LA, Criado JM. Accuracy of Senum and Yang's approximations to the Arrhenius integral. J Therm Anal Calorim 2000;60:909–15. doi:10.1023/A:1010115926340.

[41] Habschied K, Živković A, Krstanović V, Mastanjević K. Functional Beer—A Review on Possibilities. Beverages 2020;6:51. doi:10.3390/beverages6030051.

[42] Parr H, Bolat I, Cook D. Modelling flavour formation in roasted malt substrates under controlled conditions of time and temperature. Food Chem 2021;337:127641. doi:10.1016/j.foodchem.2020.127641.

[43] Windes S, Bettenhausen HM, Simaeys KRV, Clawson J, Fisk S, Heuberger AL, et al. Comprehensive Analysis of Different Contemporary Barley Genotypes Enhances and Expands the Scope of Barley Contributions to Beer Flavor. J Am Soc Brew Chem 2020:1–25. doi:10.1080/03610470.2020.1843964.

[44] Vassilev S V., Baxter D, Andersen LK, Vassileva CG. An overview of the chemical composition of biomass. Fuel 2010;89:913–33. doi:10.1016/J.FUEL.2009.10.022.

[45] Channiwala SA, Parikh PP. A unified correlation for estimating HHV of solid, liquid and gaseous fuels. Fuel 2002;81:1051–63. doi:10.1016/S0016-2361(01)00131-4.

[46] Vanreppelen K, Vanderheyden S, Kuppens T, Schreurs S, Yperman J, Carleer R. Activated carbon from pyrolysis of brewer's spent grain: Production and adsorption properties. Waste Manag Res 2014;32:634–45. doi:10.1177/0734242X14538306.

[47] Amutio M, Lopez G, Aguado R, Artetxe M, Bilbao J, Olazar M. Kinetic study of lignocellulosic biomass oxidative pyrolysis. Fuel 2012;95:305–11. doi:10.1016/J.FUEL.2011.10.008.

[48] Coronado MA, Montero G, Montes DG, Valdez-Salas B, Ayala JR, García C, et al. Physicochemical characterization and SEM-EDX analysis of brewer's spent grain from the craft brewery industry. Sustain 2020;12. doi:10.3390/su12187744.

[49] Shen DK, Gu S, Luo KH, Bridgwater A V., Fang MX. Kinetic study on thermal decomposition of woods in oxidative environment. Fuel 2009;88:1024–30. doi:10.1016/j.fuel.2008.10.034.

[50] Yao F, Wu Q, Lei Y, Guo W, Xu Y. Thermal decomposition kinetics of natural fibers: Activation energy with dynamic thermogravimetric analysis. Polym Degrad Stab 2008;93:90–8. doi:10.1016/j.polymdegradstab.2007.10.012.

[51] Mishra G, Bhaskar T. Non isothermal model free kinetics for pyrolysis of rice straw. Bioresour Technol 2014;169:614–21. doi:10.1016/j.biortech.2014.07.045.

[52] Bi H, Wang C, Lin Q, Jiang X, Jiang C, Bao L. Combustion behavior, kinetics, gas emission characteristics and artificial neural network modeling of coal gangue and biomass via TG-FTIR. Energy 2020;213:118790. doi:10.1016/j.energy.2020.118790.

[53] Wang Q, Wang G, Zhang J, Lee JY, Wang H, Wang C. Combustion behaviors and kinetics analysis of coal, biomass and plastic. Thermochim Acta 2018;669:140–8. doi:10.1016/j.tca.2018.09.016.

[54] Singh R, Krishna BB, Mishra G, Kumar J, Bhaskar T. Strategies for selection of thermo-chemical processes for the valorisation of biomass. Renew Energy 2016;98:226–37. doi:10.1016/j.renene.2016.03.023.

[55] Badía Valiente JD. Strategies and analytical procedures for a sustainable plastic waste management. An application to poly (ethylene terephthalate) and polylactide in the packaging sector. Universitat Politècnica de València, 2011.

[56] López-González D, Fernandez-Lopez M, Valverde JL, Sanchez-Silva L. Thermogravimetric-mass spectrometric analysis on combustion of lignocellulosic biomass. Bioresour Technol 2013;143:562–74. doi:10.1016/j.biortech.2013.06.052.

[57] Khawan A, Flangan DR, Khawam A, Flanagan DR. Solid-state kinetic models: Basics and mathematical fundamentals. J Phys Chem B 2006;110:17315–28. doi:10.1021/jp062746a.

[58] IEA Bioenergy. Emerging Gasification Technologies for Waste & Biomass. 2020.

[59] James AK, Thring RW, Helle S, Ghuman HS. Ash management review-applications of biomass bottom ash. Energies 2012;5:3856–73. doi:10.3390/en5103856.

[60] Salinas CT, Pu Y, Lou C, dos Santos DB. Experiments for combustion temperature measurements in a sugarcane bagasse large-scale boiler furnace. Appl Therm Eng 2020;175:115433. doi:10.1016/j.applthermaleng.2020.115433.

[61] Kleinhans U, Wieland C, Frandsen FJ, Spliethoff H. Ash formation and deposition in coal and biomass fired combustion systems: Progress and challenges in the field of ash particle sticking and rebound behavior. Prog Energy Combust Sci 2018;68:65–168. doi:10.1016/j.pecs.2018.02.001.

O. Gil-Castell, N. Mascia, C. Primaz, F. Vásquez-Garay, M.G. Baschetti, A. Ribes-Greus. Brewer's spent grains as biofuels in combustion-based energy recovery processes: Evaluation of thermo-oxidative decomposition. Fuel, 2022; 312(122955)

ANNEX – OPEN ACCESS POLICIES